2003-01-1710

Estimation of Dynamic Stiffness Matrix of Welded or Glued Joints Using a Laboratory Fixture

Pavak Mehta and Rajendra Singh
Center for Automotive Research, The Ohio State University

ABSTRACT

Accurate quantification of welded or adhesive joints in automotive chassis structures is necessary before reliable models can be developed. Such joints undergo shear and rotational deformations, which must be characterized via diagonal stiffness elements and cross-stiffness terms in order to describe static and dynamic problems. In this paper, a frequency domain decomposition technique is employed to extract static stiffness and viscous damping matrices of dimension 2 via analytical, computational or experimental models. Methods are applied to a laboratory fixture and alternate joints are compared.

INTRODUCTION

For a real-life structure (such as the vehicle chassis) that may posses numerous welded (or adhesive) joints, it is very difficult to assess the joint static stiffness and damping properties [1-3]. Lack of understanding of joint mechanisms leads to either detailed models that must be iteratively solved using finite element methods or gross approximations based on intuition. Hence, some effort has gone into developing experimental techniques that could extract joint properties from an assembled structure [3-11]. Techniques proposed in the literature [4-10] deal with the measurement of vibrational data on an assembled structure, but most of these techniques do not include the measurement of rotational stiffness term. Wang and Liou [4] proposed a technique to backtrack joint properties from the measured frequency response functions (FRFs), but the method is valid only for a laboratory structure with discrete one-dimensional joints. Also, some researchers have proposed algorithms and mathematical tools to overcome the ill-conditioning of FRF matrices. For instance, Ren and Beards [2] have suggested techniques for reducing experimental signal errors and matrix ill-conditioning problems. Their method works well for a multi-dimensional beam system with some restrictions. They also have developed theoretical and experimental methods to estimate FRFs from inaccessible points [5, 6]. But, the rotational degrees of freedom are not considered. Liu and Ewins [7-8] proposed a theoretical technique to extract joint mass, damping and stiffness, suggesting the use of a partitioning algorithm to condition the FRF matrix. Chen et. al. [9] used relationship between measured FRFs of the complex valued eigenvectors to extract normal modes for highly damped systems and proposed frequency domain technique to extract mass, stiffness and damping matrices. A practical and yet repeatable technique for extracting diagonal, rotational and cross coupling terms from measured FRFs was proposed by Young et. al. [3]. Using the proposed frequency domain decomposition technique, static stiffnesses related to joint's shear deformation, rotational deformation and cross coupling terms were successfully extracted for a well-designed laboratory experiment with bolted or integral joints [3].

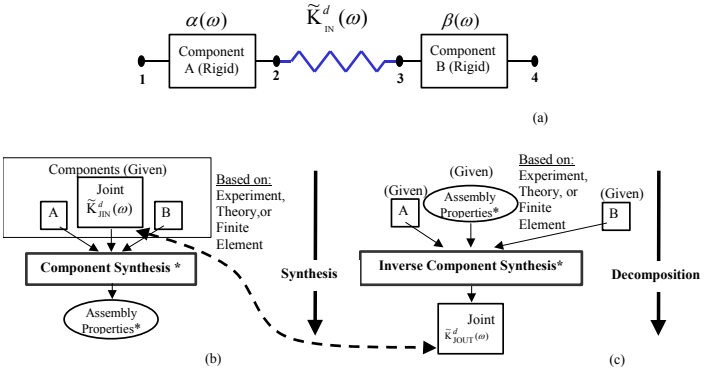

Figure 1. Summary of proposed method. (a) Assembly consisting of two rigid blocks and elastic joint. (b) Synthesis process where dynamic property of the assembly is the output. (c) Decomposition process where dynamic property of the joint is the output.

Chief objective of this paper is to present advancements made to Young's method [3]. Specifically, we intend to extract the dynamic stiffness matrix associated with the fixture of Figure 1. The assembly consists of two rigid steel blocks connected by an elastic joint, which includes an elastic beam and two interfaces at point 2 and 3 Specifically, joint could be viewed as a combination of three damped springs in series; the middle spring represents an elastic beam and two end springs describe interfaces where integral, welded or glued

joints exists (Figure 2b). The static stiffness matrix associated with the elastic beam (E) is derived using the Euler's beam theory [3]. The dynamic stiffness matrix associated with the interfaces is extracted using experimental data and the decomposition method. Overall, stiffness matrices of elastic joint with integral, weld or glue (epoxy) interfaces are obtained and analyzed.

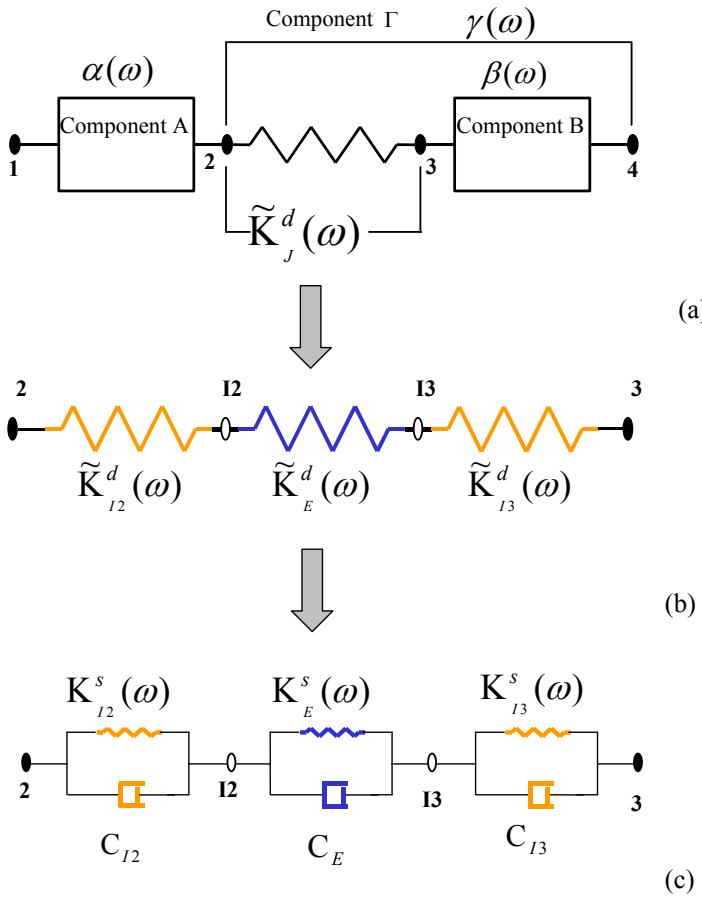

Figure 2. Component mobility synthesis or decomposition concept. (a) Components and compliance. (b) Three damped springs in series describing joint stiffness. (c) Model of damped springs based on the Voigt model assumption.

Our experiments are carried out using the LMS Cada-X impact test and modal analysis software [12], running on a Hewlett Packard UNIX workstation [13] with a multi-channel Agilent front-end [14]. This software calculates modal damping ratios based on multiple FRFs. Lumped analytical model is executed with the MATLAB [15] and the MAPLE [16] while the finite element method is implemented using the ANSYS [17] software. Refer to the companion article [18] for key examples with alternate joints that will be used in this paper.

COMPONENT MOBILITY SYNTHESIS AND DECOMPOSITION TECHNIQUE

The dynamic behavior of the assembled structure can be obtained by synthesizing the FRFs of individual components of an assembly. Here, the assembly consists of an elastic joint (J) and two rigid blocks (A and B) of Figure 1a. We employ the mobility or dynamic compliance synthesis method as shown in Figure 1b [16, 12, 3]. Utilizing FRFs of an assembled structure, dynamic properties of an individual component can be derived using the decomposition technique, Figure 1c [3]. Three approaches are employed to obtain the complex valued compliance of an assembly, namely the analytical (SIM), experimental (EXP) and computational (FEM) methods. The dynamic compliances of individual blocks A and B are calculated using only the SIM method. Known or input joint properties used in the synthesis technique are denoted by the subscript 'IN' and the joint property extracted using the decomposition technique is labeled with the subscript 'OUT'. Each joint (J) here is assumed to be a massless elastic link given in terms of dynamic stiffness $\tilde{K}^d_J(\omega)$ that includes spectrally-varying static stiffness $K^s_J(\omega)$ and viscous damping C_J, where ω is the frequency of excitation in rad/s.

$$\tilde{K}^d_J(\omega) = K^s_J(\omega) + i\omega C_J(\omega) \qquad (1)$$

Sub-structure models are coupled by enforcing motion–compatibility and force-equilibrium conditions at attachment points common to the mating sub-structures [19]. In this study, dynamic compliance-like FRFs are used. As an illustration of how the component synthesis technique is used to couple sub-structures, consider an elastic joint (J) and two rigid blocks (A and B) with single DOFs at input and output terminals (Figure 2a). Point 1 and 4 represents input and output DOFs of overall system. Here, the goal of mobility synthesis is to relate input force ($\tilde{F}_1(\omega)$) at point 1 and displacement response ($\tilde{Y}_4(\omega)$) at point 4. Assumptions for the model are (a) Elastic joint (J) includes elastic beam (E) and two interfaces (I2 and I3) at point 2 and 3 respectively and (b) Elastic joint (J) is an equivalent dynamic spring ($\tilde{K}^d_J(\omega)$) corresponding three dynamic springs in series. Here, the end springs ($K^s_{I2}(\omega)$ and $K^s_{I3}(\omega)$) represent interfaces and the middle spring represents the elastic beam stiffness ($K^s_E(\omega)$) as shown in Figure 2b. Dynamic spring is modeled using the Voigt visco-elastic model [19,20], which is a parallel arrangement of $K^s_J(\omega)$ and $C_J(\omega)$ (Figure 2c).

The harmonic displacement amplitude $\tilde{Y}_i(\omega)$ at any point of interest on a given component can be expressed in terms of driving-point compliance $\tilde{H}_{ii}(\omega)$ and cross-point compliance $\tilde{H}_{ij}(\omega)$, when the harmonic forces are applied at the driving-point $\tilde{F}_i(\omega)$ and at the cross point adjacent to it $\tilde{F}_j(\omega)$ (equation 2). Note all variables are complex valued and function of frequency ω.

$$\widetilde{\mathrm{Y}}_i(\omega) = \widetilde{\mathrm{F}}_i(\omega)\widetilde{\mathrm{H}}_{ii}(\omega) + \widetilde{\mathrm{F}}_j(\omega)\widetilde{\mathrm{H}}_{ij}(\omega) \qquad (2)$$

Considering components A and B of Figure 2a individually, equations (3a-b) define, $\alpha_{ii}(\omega)$ and $\beta_{ii}(\omega)$ as the driving-point, $\alpha_{ij}(\omega)$ and $\beta_{ij}(\omega)$ as the cross-point compliances for components A and B respectively.

$$\begin{Bmatrix} \widetilde{\mathrm{Y}}_1(\omega) \\ \widetilde{\mathrm{Y}}_2(\omega) \end{Bmatrix} = \begin{bmatrix} \alpha_{11}(\omega) & \alpha_{12}(\omega) \\ \alpha_{21}(\omega) & \alpha_{22}(\omega) \end{bmatrix} \begin{Bmatrix} \widetilde{\mathrm{F}}_1(\omega) \\ \widetilde{\mathrm{F}}_2(\omega) \end{Bmatrix} \qquad (3a)$$

$$\begin{Bmatrix} \widetilde{\mathrm{Y}}_3(\omega) \\ \widetilde{\mathrm{Y}}_4(\omega) \end{Bmatrix} = \begin{bmatrix} \beta_{33}(\omega) & \beta_{34}(\omega) \\ \beta_{43}(\omega) & \beta_{44}(\omega) \end{bmatrix} \begin{Bmatrix} \widetilde{\mathrm{F}}_3(\omega) \\ \widetilde{\mathrm{F}}_4(\omega) \end{Bmatrix} \qquad (3b)$$

Dynamic compliance matrix relating terminals 1 and 4 are derived as [3].

$$\widetilde{\mathrm{Y}}_4(\omega) = \beta_{43}(\omega)\frac{1}{\alpha_{22}(\omega) + 1/\widetilde{\mathrm{K}}_J^d(\omega) + \beta_{33}(\omega)}\alpha_{21}(\omega)\widetilde{\mathrm{F}}_1(\omega) \qquad (4)$$

Thus, the joint dynamic stiffness $\widetilde{\mathrm{K}}_J^d(\omega)$ is

$$1/\widetilde{\mathrm{K}}_J^d(\omega) = \left(\alpha_{21}(\omega)\frac{1}{\widetilde{\mathrm{H}}_{41}(\omega)}\beta_{43}(\omega) - \alpha_{22}(\omega) - \beta_{33}(\omega)\right) \qquad (5)$$

To extract the interface stiffness, joint dynamic stiffness is resolved into three dynamic stiffnesses (Figure 2b) in series, as shown below.

$$\frac{1}{\widetilde{\mathrm{K}}_J^d(\omega)} = \frac{1}{\widetilde{\mathrm{K}}_{12}^d(\omega)} + \frac{1}{\widetilde{\mathrm{K}}_{\mathrm{E}}^d(\omega)} + \frac{1}{\widetilde{\mathrm{K}}_{13}^d(\omega)} \qquad (6)$$

This equation is valid for a scalar problem. For a multidimensional case, equation (5) is rewritten in a matrix form as

$$\widetilde{\mathbf{K}}_J^d(\omega) = \left[\boldsymbol{\alpha}_{21}(\omega)\widetilde{\mathbf{H}}_{41}{}^{-1}(\omega)\boldsymbol{\beta}_{43}(\omega) - \boldsymbol{\alpha}_{22}(\omega) - \boldsymbol{\beta}_{33}(\omega)\right]^{-1} \qquad (7)$$

In order to extract dynamic stiffness matrix related to elastic joint using equation (7), individual component compliance matrices and assembly compliance matrix on the right hand side of equation (7) are required. Three approaches (SIM, EXP and FEM) are employed for this purpose. Table 1 indicates the source of compliance matrices for three models. Also, input and output properties of the joint are tabulated.

ANALYTICAL MODEL (SIM)

Driving point compliance $\boldsymbol{\alpha}_{22}(\omega)$ of rigid component A is a function of its mass matrix only where the excitation and response locations are same (point 2). The cross point compliance $\boldsymbol{\alpha}_{21}(\omega)$ is calculated by transferring force and moment excitation from output point 2 to input point 1. Note that the transverse and rotational response magnitudes are calculated at output location 2, as shown in equation (9) [3].

$$\boldsymbol{\alpha}_{22}(\omega) = \begin{bmatrix} \widetilde{\mathrm{Y}}_2/\widetilde{\mathrm{F}}_2 & \widetilde{\mathrm{Y}}_2/\widetilde{\mathrm{Q}}_2 \\ \widetilde{\Theta}_2/\widetilde{\mathrm{F}}_2 & \widetilde{\Theta}_2/\widetilde{\mathrm{Q}}_2 \end{bmatrix}(\omega) = (-\omega^2\mathbf{M}_A)^{-1}\begin{bmatrix} 1 & 0 \\ 0 & 1 \end{bmatrix} \qquad (8)$$

$$\boldsymbol{\alpha}_{21}(\omega) = \begin{bmatrix} \widetilde{\mathrm{Y}}_2/\widetilde{\mathrm{F}}_1 & \widetilde{\mathrm{Y}}_2/\widetilde{\mathrm{Q}}_1 \\ \widetilde{\Theta}_2/\widetilde{\mathrm{F}}_1 & \widetilde{\Theta}_2/\widetilde{\mathrm{Q}}_1 \end{bmatrix}(\omega) = (-\omega^2\mathbf{M}_A)^{-1}\begin{bmatrix} 1 & 0 \\ -\ell_A & 1 \end{bmatrix} \qquad (9)$$

Similarly the driving point compliance $\boldsymbol{\beta}_{33}(\omega)$ of rigid component B is given by equation (10) as shown below.

$$\boldsymbol{\beta}_{33}(\omega) = \begin{bmatrix} \widetilde{\mathrm{Y}}_3/\widetilde{\mathrm{F}}_3 & \widetilde{\mathrm{Y}}_3/\widetilde{\mathrm{Q}}_3 \\ \widetilde{\Theta}_3/\widetilde{\mathrm{F}}_3 & \widetilde{\Theta}_3/\widetilde{\mathrm{Q}}_3 \end{bmatrix}(\omega) = (-\omega^2\mathbf{M}_B)^{-1}\begin{bmatrix} 1 & 0 \\ 0 & 1 \end{bmatrix} \qquad (10)$$

The cross compliance $\boldsymbol{\beta}_{43}(\omega)$ is calculated by shifting response to location 4 and keeping the excitation at 3, as shown below.

$$\boldsymbol{\beta}_{43}(\omega) = \begin{bmatrix} \widetilde{\mathrm{Y}}_4/\widetilde{\mathrm{F}}_3 & \widetilde{\mathrm{Y}}_4/\widetilde{\mathrm{Q}}_3 \\ \widetilde{\Theta}_4/\widetilde{\mathrm{F}}_3 & \widetilde{\Theta}_4/\widetilde{\mathrm{Q}}_3 \end{bmatrix}(\omega) = \boldsymbol{\Delta}^{-1}\begin{bmatrix} 1 & 0 \\ 0 & 1 \end{bmatrix} \qquad (11)$$

where,

$$\boldsymbol{\Delta}(\omega) = (-\omega^2\mathbf{M}_B)\begin{Bmatrix} \widetilde{\mathrm{Y}}_4 - \ell_B\widetilde{\Theta}_4 \\ \widetilde{\Theta}_4 \end{Bmatrix} \qquad (12)$$

Individual compliance matrices thus obtained are used for the decomposition technique in EXP and FEM models as well. Combining the assembly's mass matrix, $\mathbf{M}$, and static stiffness matrix $\mathbf{K}_E^s$ the dynamic stiffness matrix $\widetilde{\mathbf{D}}(\omega)$ of an undamped LTI system is [18]

$$\widetilde{\mathbf{D}}(\omega) = -\omega^2\mathbf{M} + \mathbf{K}_E^s \qquad (13a)$$

$$\widetilde{\mathbf{D}}(\omega)\begin{Bmatrix} \widetilde{\mathrm{Y}}_2 \\ \widetilde{\Theta}_2 \\ \widetilde{\mathrm{Y}}_3 \\ \widetilde{\Theta}_3 \end{Bmatrix} = \begin{Bmatrix} \widetilde{\mathrm{F}}_2 \\ \widetilde{\mathrm{Q}}_2 \\ \widetilde{\mathrm{F}}_3 \\ \widetilde{\mathrm{Q}}_3 \end{Bmatrix} \qquad (13b)$$

In addition, if the assembly posses damping then $\widetilde{\mathbf{D}}(\omega)$ is rewritten as follows, where $\widetilde{\mathbf{K}}_J^d(\omega)$ is dynamic stiffness matrix.

$$\widetilde{\mathbf{D}}(\omega) = -\omega^2\mathbf{M} + \widetilde{\mathbf{K}}_J^d(\omega) \qquad (14)$$

Assuming Rayleigh type viscous damping, we get

Model and key	Components				Assembly	Joint Properties			
	α_{21}	α_{22}	β_{33}	β_{43}	$\widetilde{\mathbf{H}}_{41}(\omega)$	$\widetilde{\mathbf{K}}^{d}_{JIN}(\omega)$		$\widetilde{\mathbf{K}}^{d}_{JOUT}(\omega)$	
						$\mathbf{K}^{s}_{J}$	$\mathbf{C}_{J}$	$\mathbf{K}^{s}_{J}$	$\mathbf{C}_{J}$
Analytical (SIM)	SIM				SIM	✔	✔	✔	✔
Experimental (EXP)	SIM				EXP			✔	✔
Computational (FEM)	SIM				FEM		✔	✔	✔

Table 1. Summary of three models used for the decomposition technique.

Example	Type	Asymptotic static stiffnesses of diagonal elements of $\mathbf{K}^{sa}_{J} = \mathbf{K}^{sa}_{\mathrm{OUT}}$					
		$\mathrm{K}^{sa}_{\mathrm{FyOUT}}$ (MN/m) (1,1)			$\mathrm{K}^{sa}_{\mathrm{Q}\theta\mathrm{OUT}}$ (kNm/rad) (2,2)		
		SIM	EXP	FEM	SIM	EXP	FEM
D0	Integral	3.3	4.0	3.6	3.5	4.0	12.0
E0		3.8	---	3.9	9.7	---	8.0
E1	Welded	---	0.9	1.0	---	0.6	2.3
E2		---	0.7	0.7	---	1.9	4.1
E3		---	3.4	2.9	---	3.1	13.2
E4		---	1.3	1.0	---	2.6	2.3
E5		---	4.2	4.1	---	8.5	12.2
F01	Integral	25.1	14.9	12.4	2.8	10.2	13.7
F1	Glued	---	0.8	---	---	0.61	---
F02	Integral	0.5	0.5	0.4	0.1	0.1	0.1
F2	Glued	---	0.5	---	---	0.2	---

Table 2. Extracted stiffness values of the diagonal elements $\mathrm{K}^{sa}_{\mathrm{FyOUT}}$ and $\mathrm{K}^{sa}_{\mathrm{Q}\theta\mathrm{OUT}}$.

Example	Type	Asymptotic static stiffnesses of off-diagonal elements of $\mathbf{K}^{sa}_{J} = \mathbf{K}^{sa}_{\mathrm{OUT}}$					
		$\mathrm{K}^{sa}_{\mathrm{F}\theta\mathrm{OUT}}$ (kN/rad) (1,2)			$\mathrm{K}^{sa}_{\mathrm{QyOUT}}$ (kNm/m) (2,1)		
		SIM	EXP	FEM	SIM	EXP	FEM
D0	Integral	107.9	109.5	83.1	105.5	106.6	113.1
E0		141.2	---	68.2	141.2	---	129.2
E1	Welded	---	22.4	20.1	---	11.2	30.0
E2		---	17.0	10.9	---	9.9	17.0
E3		---	53.4	54.6	---	73.6	98.3
E4		---	12.8	10.6	---	23.4	22.7
E5		---	122.0	96.9	---	56	131.4
F01	Integral	308.6	138.1	243.2	308.6	136.5	243.2
F1	Glued	---	47.8	---	---	45.4	---
F02	Integral	4.7	5.0	2.1	4.7	4.1	3.9
F2	Glued	---	4.8	---	---	2.5	---

Table 3. Extracted stiffness values of the off-diagonal elements $\mathrm{K}^{sa}_{\mathrm{F}\theta\mathrm{OUT}}$ and $\mathrm{K}^{sa}_{\mathrm{QyOUT}}$.

$$\widetilde{\mathbf{K}}_J^d(\omega) = \mathbf{K}_J^s(\omega) + i\omega\mathbf{C}_J(\omega) \tag{15}$$

$$\mathbf{C}_J(\omega) = \mathrm{C}_m\mathbf{M} + \mathrm{C}_k\mathbf{K}_J^s(\omega) \tag{16}$$

Where, C_m and C_k are proportionality constants (scalar). If the visco-elastic type proportional damping matrix is assumed, then redefine $\widetilde{\mathbf{K}}_J^d(\omega)$ as follows, where η is a scalar loss factor.

$$\widetilde{\mathbf{K}}_J^d(\omega) = \mathbf{K}_J^s(1+i\eta)(\omega) \tag{17}$$

In the analytical (SIM) model, proportional viscous damping is assumed and joint viscous damping matrix $\mathbf{C}_J(\omega)$ is constructed from measured modal damping ratios (ζ_r), as explained in a later section. Hence equations (12) and (17) define the system. Since we want to find the complex valued $\widetilde{\mathbf{H}}_{41}(\omega)$, response calculated at point 3 is shifted to point 4 and the applied excitation is shifted from point 2 to point 1 in equation (13). With this transformation of coordinates and applying $\widetilde{\mathrm{Y}}_3(\omega) = \widetilde{\mathrm{Y}}_4(\omega) - \ell_B\widetilde{\Theta}_4(\omega)$ and $\widetilde{\Theta}_3(\omega) = \widetilde{\Theta}_4(\omega)$ to equation (13), results in a modified dynamic stiffness matrix $\widetilde{\mathbf{D}}_{\mathrm{mod}}(\omega)$.

$$\begin{bmatrix} \begin{bmatrix} \widetilde{\mathrm{Y}}_1/\widetilde{\mathrm{F}}_1 & \widetilde{\mathrm{Y}}_2/\widetilde{\mathrm{Q}}_1 \\ \widetilde{\Theta}_2/\widetilde{\mathrm{F}}_1 & \widetilde{\Theta}_2/\widetilde{\mathrm{Q}}_1 \end{bmatrix}_{2\times2} \\ \begin{bmatrix} \widetilde{\mathrm{Y}}_4/\widetilde{\mathrm{F}}_1 & \widetilde{\mathrm{Y}}_4/\widetilde{\mathrm{Q}}_1 \\ \widetilde{\Theta}_4/\widetilde{\mathrm{F}}_1 & \widetilde{\Theta}_4/\widetilde{\mathrm{Q}}_1 \end{bmatrix}_{2\times2} \end{bmatrix}_{4\times2} (\omega) = \left[\widetilde{\mathbf{D}}_{\mathrm{mod}}(\omega)\right]^{-1} \begin{bmatrix} 1 & 0 \\ -\ell_A & 1 \\ 0 & 0 \\ 0 & 0 \end{bmatrix} \tag{18}$$

The left hand side matrix in equation (18) has dimensions of 4×2 but the lower 2×2 matrix is the required $\widetilde{\mathbf{H}}_{41}(\omega)$ matrix [3]. Notice that mass, stiffness and damping matrices are 4×4, and that the dynamic stiffness matrix derived from them is 2×2. Next, $\widetilde{\mathbf{K}}_J^d(\omega)$ is extracted by equations (7-11) and (18). Using the MAPLE [16] software, symbolic expressions for $\boldsymbol{\alpha}_{21}(\omega)$, $\boldsymbol{\alpha}_{22}(\omega)$, $\boldsymbol{\beta}_{33}(\omega)$, $\boldsymbol{\beta}_{43}(\omega)$, $\widetilde{\mathbf{H}}_{41}(\omega)$ and $\widetilde{\mathbf{K}}_J^d(\omega)$ are derived and used to calculate numerical values for all SIM models corresponding to Examples D0, E0, F01 and F02.

EXPERIMENTAL MODEL (EXP)

To extract the joint stiffness using equation (7) in the EXP model, individual compliance matrices and assembly compliance matrix are needed. Since individual compliance matrices based on the SIM model correlate well those from EXP model [3], only the assembly compliance matrix is required. As mentioned earlier, rotational stiffness elements are needed to model the joint stiffness matrix but it is difficult to accurately measure rotational motions of a structure. For a harmonic moment excitation, two translational accelerometers are placed 'd' apart on a rigid surface as shown in Figure 3a [3]. Further, complex valued translational acceleration amplitudes, $\widetilde{\ddot{\mathrm{Y}}}_i(\omega)$ and $\widetilde{\ddot{\mathrm{Y}}}_j(\omega)$, are measured and integrating twice to yield dynamic displacements $\widetilde{\mathrm{Y}}_i(\omega)$ and $\widetilde{\mathrm{Y}}_j(\omega)$. The following yields the rotational deflection of the rigid surface in the frequency domain.

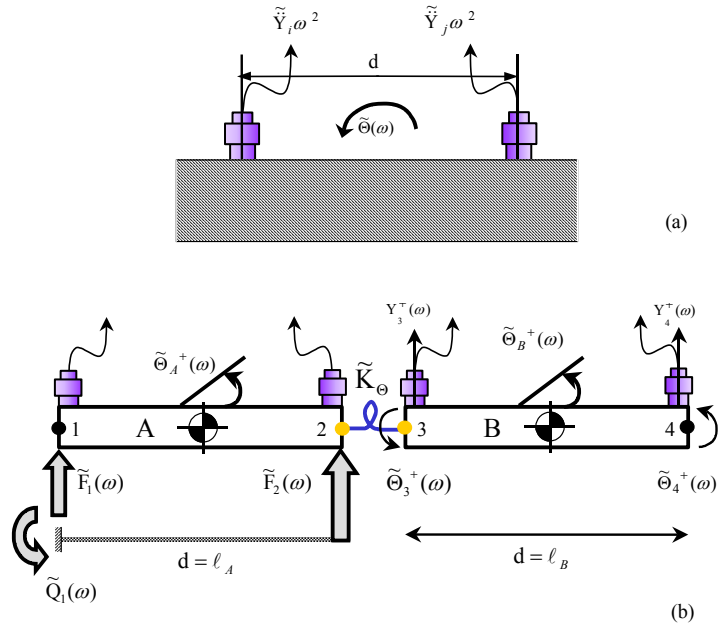

Figure 3. Experimental measurement of rotational responses. (a) Two accelerometer method. (b) Sign Conventions and the generation of harmonic moment using impulse forces.

$$\widetilde{\Theta}(\omega) = -(\widetilde{\mathrm{Y}}_j(\omega) - \widetilde{\mathrm{Y}}_i(\omega))/\mathrm{d} \tag{19}$$

For harmonic moment excitation ($\widetilde{\mathrm{Q}}(\omega) = \mathrm{d}\widetilde{\mathrm{F}}(\omega)$), an impulsive force amplitude ($\widetilde{\mathrm{F}}(\omega)$) is used at d away from the reference point (Figure 3b). Thus, the following assembly dynamic compliance and joint dynamic stiffness matrices are determined.

$$\widetilde{\mathbf{H}}_{ij}(\omega) = \begin{bmatrix} \widetilde{\mathrm{Y}}_i/\widetilde{\mathrm{F}}_j & \widetilde{\mathrm{Y}}_i/\widetilde{\mathrm{Q}}_j \\ \widetilde{\Theta}_i/\widetilde{\mathrm{F}}_j & \widetilde{\Theta}_i/\widetilde{\mathrm{Q}}_j \end{bmatrix}(\omega) \tag{20a}$$

$$\widetilde{\mathbf{K}}_{ij}(\omega) = \begin{bmatrix} \widetilde{\mathrm{F}}_j/\widetilde{\mathrm{Y}}_i & \widetilde{\mathrm{F}}_j/\widetilde{\Theta}_i \\ \widetilde{\mathrm{Q}}_j/\widetilde{\mathrm{Y}}_i & \widetilde{\mathrm{Q}}_j/\widetilde{\Theta}_i \end{bmatrix}(\omega) \tag{20b}$$

Note that $\widetilde{\mathbf{H}}_{41}(\omega)$ is two-dimensional complex matrix and its elements describe a transverse and rotational responses to force and moment excitations as shown by equation (21); refer Figure 3b for sign convention.

$$\tilde{\mathbf{H}}_{41}(\omega)=\begin{bmatrix}\tilde{Y}_4/\tilde{F}_1 & \tilde{Y}_4/\tilde{Q}_1\\ \tilde{\Theta}_4/\tilde{F}_1 & \tilde{\Theta}_4/\tilde{Q}_1\end{bmatrix}(\omega) \quad (21)$$

The following FRFs are directly measured from 0 to 1000 Hz with 2.5 Hz resolution, $\tilde{Y}_4(\omega)/\tilde{F}_1(\omega)$, $\tilde{Y}_3(\omega)/\tilde{F}_1(\omega)$, $\tilde{Y}_4(\omega)/\tilde{F}_2(\omega)$ and $\tilde{Y}_3(\omega)/\tilde{F}_2(\omega)$. The rest of (21) terms are derived as follows. Element (1,2) is calculated using equation (22) as shown in Figure 3b.

$$\left(\frac{\tilde{Y}_4}{\tilde{Q}_1}\right)=\frac{1}{\ell_A}\left[\left(\frac{\tilde{Y}_4}{\tilde{F}_2}\right)-\left(\frac{\tilde{Y}_4}{\tilde{F}_1}\right)\right] \quad (22)$$

Element (2,1) is found using equation (19) and element (2,2) is found by applying the following

$$\tilde{\mathbf{H}}_{41}(\omega)=\begin{bmatrix}\left(\frac{\tilde{Y}_4}{\tilde{F}_1}\right) & \frac{1}{\ell_A}\left[\left(\frac{\tilde{Y}_4}{\tilde{F}_2}\right)-\left(\frac{\tilde{Y}_4}{\tilde{F}_1}\right)\right]\\ \left(\frac{\tilde{\Theta}_4}{\tilde{F}_1}\right) & \frac{1}{\ell_A}\left[\left(\frac{\tilde{\Theta}_4}{\tilde{F}_2}\right)-\left(\frac{\tilde{\Theta}_4}{\tilde{F}_1}\right)\right]\end{bmatrix}(\omega) \quad (23)$$

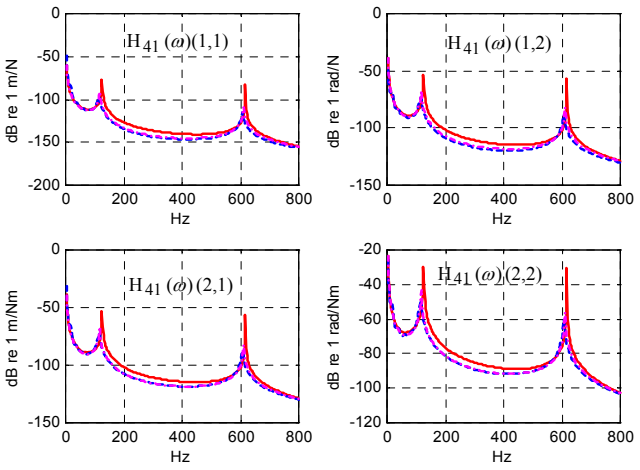

Figure 4. Comparison of H41 spectra for an integral joint (Example D0). Key: ——— SIM, ····· EXP and - - - - FEM

COMPUTATIONAL MODEL (FEM)

Finite element method model is used to validate EXP and SIM results. Like the EXP method, only $\tilde{\mathbf{H}}_{41}(\omega)$ is acquired in this model to extract $\tilde{\mathbf{K}}_J^d(\omega)$ using equation (7). From equation (23), it is clear that only four transverse FRFs, $\tilde{Y}_4(\omega)/\tilde{F}_1(\omega)$, $\tilde{Y}_3(\omega)/\tilde{F}_1(\omega)$, $\tilde{Y}_4(\omega)/\tilde{F}_2(\omega)$ and $\tilde{Y}_3(\omega)/\tilde{F}_2(\omega)$, are needed to construct $\tilde{\mathbf{H}}_{41}(\omega)$ with rotational and coupling terms. Harmonic analysis for FEM is carried out using the mode superposition method [21]. A method for incorporating measured modal damping ratios (ζ_r) in $\tilde{\mathbf{H}}_{41}(\omega)$ using mode superposition method will be explained in the next section. Key advantage of modal analysis is the choice regarding the number of system modes. In this study, all FEM models include only the first two modes of interest. Notice good co-relation of $\tilde{\mathbf{H}}_{41}(\omega)$ spectra between analytical, experimental, and computational models (Figure 4).

ESTIMATION OF JOINT DAMPING MATRICES

The only reliable information on damping as associated with the welded or glued joints that can be measured is in the form of modal damping ratios (ζ_r). Then the proportional damping matrix $\mathbf{C}_J(\omega)$ can be constructed as follows. Undamped system eigenvalues ($\boldsymbol{\lambda}_r$) and eigenvectors ($\boldsymbol{\Phi}_r$) are needed, which are calculated from the assembly mass matrix ($\mathbf{M}$) and the stiffness matrix ($\mathbf{K}_J^s$) using equation (24) [22].

$$\mathbf{K}_J^s\boldsymbol{\Phi}_r=\mathrm{diag}[\boldsymbol{\lambda}_r]\mathbf{M}\boldsymbol{\Phi}_r \quad (24)$$

The eigenvalue matrix (diag[$\boldsymbol{\lambda}$]) is of dimension 4 and square-root of diagonal elements give two rigid modes of vibration at 0 rad/s and the first two system natural frequencies (ω_r). Using the modal matrix ($\boldsymbol{\Phi}$) and equations (25a-b), define the modal mass (diag[$\mathbf{M}_r$]) and the modal stiffness (diag[$\mathbf{K}_r$]) matrices as

$$\mathrm{diag}[\mathbf{M}_r]=\boldsymbol{\Phi}^{\mathrm{T}}\mathbf{M}\boldsymbol{\Phi} \quad (25a)$$

$$\mathrm{diag}[\mathbf{K}_r]=\boldsymbol{\Phi}^{\mathrm{T}}\mathbf{K}_J^s\boldsymbol{\Phi} \quad (25b)$$

In modal domain, construct the modal viscous damping coefficient matrix diag[C_r] as

$$\mathrm{diag}[\mathrm{C}_r]=\mathrm{diag}[2\zeta_r\omega_r] \quad (26)$$

Then, the viscous damping matrix ($\mathbf{C}_J$) in the physical domain as

$$\mathbf{C}_J=(\boldsymbol{\Xi}^{\mathrm{T}})^{-1}\mathbf{C}_r(\boldsymbol{\Xi})^{-1} \quad (27)$$

Where $\boldsymbol{\Xi}$ is an orthonormal modal matrix of dimension 4, derived in equation (28) using normalizing constant (Λ_r) in (29)

$$\boldsymbol{\Xi}=\boldsymbol{\Phi}\,\mathrm{diag}[\Lambda_r] \quad (28)$$

$$\Lambda_r=1/(\mathrm{M}_r)^{1/2} \quad (29)$$

Using $\boldsymbol{\Xi}$, orthonormal modal mass and modal stiffness matrices are derived, which yield the identity and eigenvalues matrices respectively [22].

$$\text{diag}[\mathbf{M}_{\Xi}] = \boldsymbol{\Xi}^{\mathrm{T}}\mathbf{M}_{r}\boldsymbol{\Xi} = \mathbf{I} \tag{30}$$

$$\text{diag}[\mathbf{K}_{\Xi}] = \boldsymbol{\Xi}^{\mathrm{T}}\mathbf{K}_{r}\boldsymbol{\Xi} = \boldsymbol{\lambda} \tag{31}$$

Thus, $\mathbf{C}_J$ of dimension 4 is obtained in the physical domain, as associated with joint (J).

ESTIMATION OF STATIC STIFFNESS MATRICES

Extracted $\widetilde{\mathbf{K}}^{d}_{\mathrm{OUT}}(\omega)$, which represents stiffness of elastic joint (J) $\widetilde{\mathbf{K}}^{d}_{J}(\omega)$, is complex valued and frequency-variant as defined in (32) [3]. Define the real part of it as the static stiffness $\mathbf{K}^{s}_{\mathrm{OUT}}(\omega)$ as shown below.

$$\widetilde{\mathbf{K}}^{d}_{J}(\omega) = \widetilde{\mathbf{K}}^{d}_{\mathrm{OUT}}(\omega) = \begin{bmatrix} \widetilde{\mathrm{K}}^{d}_{\mathrm{FyOUT}}(\omega) & \widetilde{\mathrm{K}}^{d}_{\mathrm{F}\theta\mathrm{OUT}}(\omega) \\ \widetilde{\mathrm{K}}^{d}_{\mathrm{QyOUT}}(\omega) & \widetilde{\mathrm{K}}^{d}_{\mathrm{Q}\theta\mathrm{OUT}}(\omega) \end{bmatrix} \tag{32}$$

$$\mathrm{Re}\,[\widetilde{\mathbf{K}}^{d}_{\mathrm{OUT}}(\omega)] = \mathbf{K}^{s}_{\mathrm{OUT}}(\omega) = \begin{bmatrix} \mathrm{K}^{s}_{\mathrm{FyOUT}}(\omega) & \mathrm{K}^{s}_{\mathrm{F}\theta\mathrm{OUT}}(\omega) \\ \mathrm{K}^{s}_{\mathrm{QyOUT}}(\omega) & \mathrm{K}^{s}_{\mathrm{Q}\theta\mathrm{OUT}}(\omega) \end{bmatrix} \tag{33}$$

Each element of $[\mathbf{K}^{s}_{\mathrm{OUT}}(\omega)]$ is calculated using the singular value decomposition method [3]. For that an over-determined set of matrix equations is created and solved using MATLAB [16]. For example, to find the element $\widetilde{\mathrm{K}}^{d}_{\mathrm{FyOUT}}(\omega)$ at each frequency, equation (34) is developed. Three other equations like (34) will make a set of equations that will yield $\mathbf{K}^{s}_{\mathrm{OUT}}(\omega)$ [3].

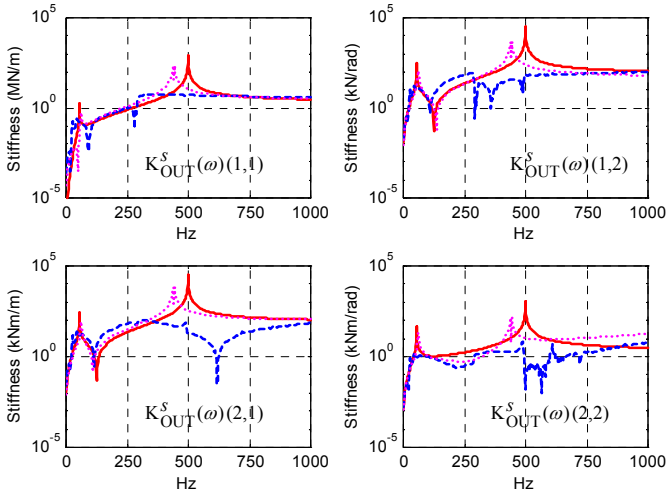

Figure 5. $\mathbf{K}^{s}_{\mathrm{OUT}}(\omega)$ spectra for an integral joint (Example D0).
Key: ——— SIM, ····· FEM and - - - - EXP

$$\begin{Bmatrix} \mathrm{K}^{s}_{\mathrm{FyOUT}}(\omega_{\min}) \\ \mathrm{K}^{s}_{\mathrm{FyOUT}}(\omega_{\min+1}) \\ \vdots \\ \mathrm{K}^{s}_{\mathrm{FyOUT}}(\omega_{\max}) \end{Bmatrix}_{(\max\times 1)} = \begin{Bmatrix} \mathrm{Re}[\widetilde{\mathrm{K}}^{d}_{\mathrm{FyOUT}}(\omega_{\min})] \\ \mathrm{Re}[\widetilde{\mathrm{K}}^{d}_{\mathrm{FyOUT}}(\omega_{\min+1})] \\ \vdots \\ \mathrm{Re}[\widetilde{\mathrm{K}}^{d}_{\mathrm{FyOUT}}(\omega_{\max})] \end{Bmatrix}_{(\max\times 1)} \tag{34}$$

Static stiffness spectra $\mathbf{K}^{s}_{\mathrm{OUT}}(\omega)$ are plotted up to a frequency little higher than second natural frequency of interest f^{2} [18]. Comparison between simulated (SIM), measured (EXP) and computed (FEM) spectra for D0 are displayed in Figure 5. Though peaks can be observed in SIM and FEM results, good agreements between SIM, FEM and EXP are noted. Noise in the measured results is explicit via elements (1,2) and (2,2), which represent stiffnesses associated with rotational deflection. There is no SIM model for Examples E1-E5 and F1-F2, hence only measured (EXP) or computed (FEM) $\mathbf{K}^{s}_{\mathrm{OUT}}(\omega)$ are available for these models. All welded or glued (epoxy) joints are compared with integral joint of same block and beam dimensions. For E1-E5, E0, for F1, F01 and for F2, F02 is an integral joint example. The $\mathbf{K}^{s}_{\mathrm{OUT}}(\omega)$ spectra for welded E2 and E5 and glued F1 are shown in Figures 6-8, respectively. Magnitudes of measured and computed $\mathbf{K}^{s}_{\mathrm{OUT}}(\omega)$ for E2 and F1 are less than simulated $\mathbf{K}^{s}_{\mathrm{OUT}}(\omega)$ for the respective integral examples. This indicates that welded or glued joint stiffness values for those particular examples are less than that of the integral joint, for all elements of the stiffness matrix. In contrast, $\mathbf{K}^{s}_{\mathrm{OUT}}(\omega)$ values for E5 are higher than that of E0 for all elements of the integral joint stiffness.

The amount of noise is noticeable in measured stiffness spectra for welded and glued (epoxy) joints. In all of the elements, stiffness spectra approach an asymptotic line. But in the stiffness spectrum, it is difficult to quantify the asymptotic value. Hence, a spectral average of stiffness for each element is taken as follows, where n represents the discrete spectral lines.

$$\mathbf{K}^{sa}_{\mathrm{OUT}} = \left\langle \mathbf{K}^{s}_{\mathrm{OUT}}(\omega) \right\rangle_{\omega} = \frac{\sum_{1}^{\mathrm{n}} \mathbf{K}^{s}_{\mathrm{OUT}}(\omega)}{\mathrm{n}} \tag{35}$$

Using equation (35), extracted stiffness matrix $\mathbf{K}^{sa}_{\mathrm{OUT}}$ at the asymptote, is derived as

$$\mathbf{K}^{sa}_{J\mathrm{OUT}} = \mathbf{K}^{sa}_{\mathrm{OUT}} = \begin{bmatrix} \left\langle \mathrm{K}^{s}_{\mathrm{FyOUT}}(\omega) \right\rangle_{\omega} & \left\langle \mathrm{K}^{s}_{\mathrm{F}\theta\mathrm{OUT}}(\omega) \right\rangle_{\omega} \\ \left\langle \mathrm{K}^{s}_{\mathrm{QyOUT}}(\omega) \right\rangle_{\omega} & \left\langle \mathrm{K}^{s}_{\mathrm{Q}\theta\mathrm{OUT}}(\omega) \right\rangle_{\omega} \end{bmatrix} \tag{36}$$

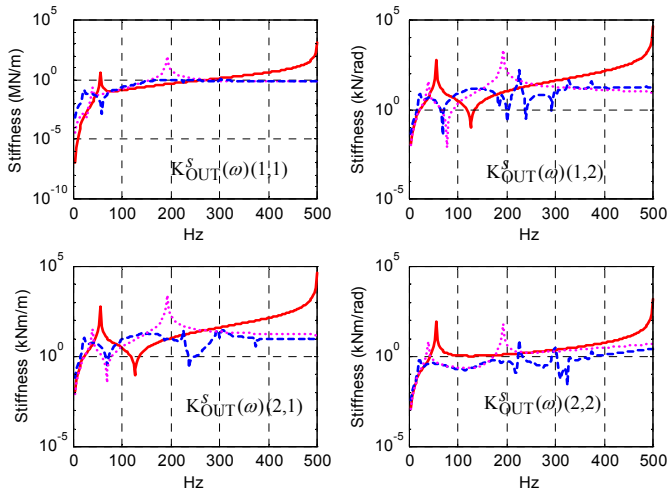

Figure 6. Comparison between measured and computed $\mathbf{K}^s_{OUT}(\omega)$ spectra of E2 and simulated $\mathbf{K}^s_{OUT}(\omega)$ spectra of E0.
Key: ——— SIM, ····· FEM and - - - - EXP

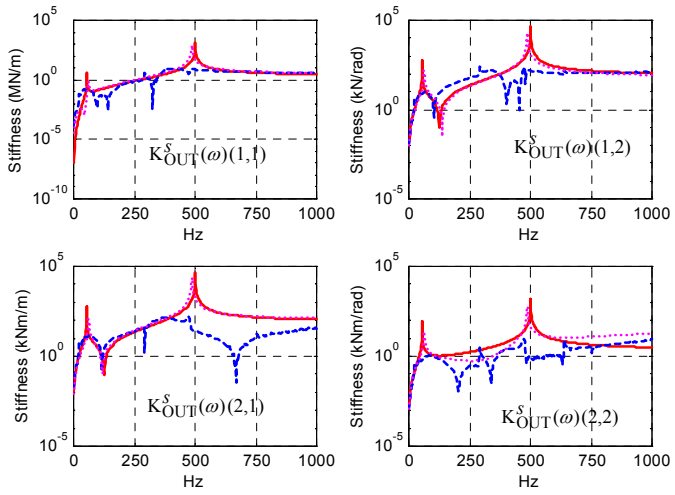

Figure 7. Comparison between measured and computed $\mathbf{K}^s_{OUT}(\omega)$ spectra of E5 and simulated $\mathbf{K}^s_{OUT}(\omega)$ spectra of E0.
Key: ——— SIM, ····· FEM and - - - - EXP.

Such stiffness values are calculated over a range (f_{min} to f_{max}), around the asymptote. Values for diagonal elements are compared in Table 2, and the values of off-diagonal terms are tabulated in Table 3. Since units of all stiffness elements are different, they cannot be compared with each other. Hence, comparison is carried out between elements of alternate joints. Examples with similar beam and block dimensions are compared with each other such as, D0 with E0–E5, F01 with F1, and F02 with F2. Looking at values of each stiffness element separately, for D0, E0-E5, F01, F02, F1 and F2, good agreement between simulated, measured and computed results are noticed especially for $K^{sa}_{F\theta OUT}$ element. Some deviation is noticed in rotational stiffness element $K^{sa}_{Q\theta OUT}$. This is due to reason that the technique used here for measuring rotational deflection is based on indirect measurements. Unrelated noise and numerical errors in finding rotational deflection introduce errors. Further, by arranging the alternate joints in an ascending order of $\mathbf{K}^{sa}_{OUT}$ stiffness magnitude, one could infer which joint is most compliant or most stiff as shown in Table 4. Among D0 and E0-E5, it is clear that E2 is the most compliant joint for elements K^{sa}_{FyOUT} and K^{sa}_{QyOUT}, while E5 is the most stiff joint for K^{sa}_{FyOUT} and $K^{sa}_{Q\theta OUT}$ respectively. This unexpected result indicates that welded joint of E5 is stiffer than the integral joint E0. Between F1 and F01, F1 is compliant and F01 is stiffer as expected.

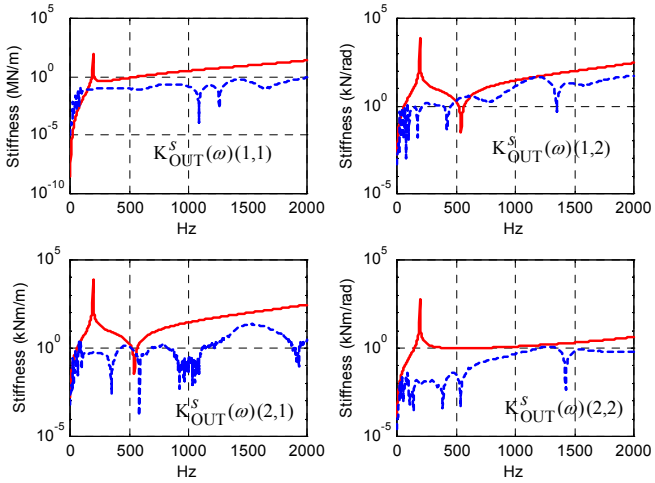

Figure 8. Comparison between measured and computed $\mathbf{K}^s_{OUT}(\omega)$ spectra of F1 and simulated $\mathbf{K}^s_{OUT}(\omega)$ spectra of F01. Key: ——— F01 and - - - - F1.

ESTIMATION OF VISCOUS DAMPING MATRICES

Define the imaginary part of extracted stiffness spectra $\tilde{\mathbf{K}}^d_{OUT}(\omega)$ from equation (37).

$$\tilde{\mathbf{K}}^d_J(\omega) = \tilde{\mathbf{K}}^d_{OUT}(\omega) = \mathrm{Re}[\tilde{\mathbf{K}}^d_{OUT}(\omega)] + \mathrm{Im}[\tilde{\mathbf{K}}^d_{OUT}(\omega)] \qquad (37)$$

Since $\tilde{\mathbf{K}}^d_{OUT}(\omega)$ is assumed to posses the Rayleigh type damping (16) $\mathbf{C}_{OUT}(\omega)$ is given by a proportionally damped matrix.

$$\mathrm{Im}[\tilde{\mathbf{K}}^d_{OUT}(\omega)] = \omega \mathbf{C}_{OUT}(\omega) = \omega \begin{bmatrix} C_{FyOUT}(\omega) & C_{F\theta OUT}(\omega) \\ C_{QyOUT}(\omega) & C_{Q\theta OUT}(\omega) \end{bmatrix} \qquad (38)$$

Each element of $\mathbf{C}_{OUT}(\omega)$ is calculated using the singular value decomposition method [3], as described in previous section for $\mathbf{K}^s_{OUT}(\omega)$. For example, to obtain the elements $C_{FyOUT}(\omega)$, equation (39) is used. Such

Rank (Ascending Order)	Example #				Model used to compare values			
	K^{sa}_{FyOUT} (1,1)	$K^{sa}_{F\theta OUT}$ (1,2)	K^{sa}_{QyOUT} (2,1)	$K^{sa}_{Q\theta OUT}$ (2,2)	K^{sa}_{FyOUT} (1,1)	$K^{sa}_{F\theta OUT}$ (1,2)	K^{sa}_{QyOUT} (2,1)	$K^{sa}_{Q\theta OUT}$ (2,2)
1 (Most Compliant)	E2	E4	E2	E1	❷,❸	❷,❸	❷,❸	❷,❸
2	E1	E2	E1	E2	❷,❸	❷,❸	❷	❷,❸
3	E4	E1	E4	E4	❷,❸	❷,❸	❷,❸	❷
4	E3	E3	E3	E3	❷,❸	❷,❸	❷,❸	❷
5	D0	D0	D0	D0	❶,❷,❸	❶,❷,❸	❶,❷,❸	❷,❸
6	E0	E5	E5	E0	❶,❸	❷,❸	❸	❸
7 (Most Stiff)	E5	E0	E0	E5	❷,❸	❶	❶,❸	❷
1 (Comp-liant)	F1	F1	F1	F1	❷	❷	❷	❷
2 (Stiff)	F01	F01	F01	F01	❶,❷,❸	❶,❷,❸	❶,❷,❸	❶,❷,❸
1 (Comp-liant)	F02	F2	F2	F02	❶,❷,❸	❷	❷	❶,❷,❸
2 (Stiff)	F2	F02	F02	F2	❷	❶,❷,❸	❶,❷,❸	❷

Table 4. Rank order of stiffness magnitures correspoinding to the elements of the extracted static stiffness matrix $\mathbf{K}^{sa}_{OUT}$.
Key: ❶= SIM, ❷ = EXP, ❸= FEM.

Example	Type	Asymptotic viscous damping of diagonal elements of $\mathbf{C}^a_J = \mathbf{C}^a_{OUT}$					
		C^a_{FyOUT} (N-s/m) (1,1)			$C^a_{Q\theta OUT}$ (Nm-s) (2,2)		
		C_{IN}	SIM	FEM	C_{IN}	SIM	FEM
D0	Integral	1.5	2.4	2.4	0.03	0.03	0.03
E1	Welded	3.2	6.3	2.0	0.02	0.2	0.02
E2		1.7	2.6	0.8	0.04	0.04	0.02
E3		1.3	2.0	1.8	0.005	0.005	0.005
E4		2.2	3.4	1.3	0.03	0.03	0.02
E5		0.9	1.0	1.5	0.03	0.04	0.04
F01	Integral	8.9	18.4	16.7	0.003	0.002	0.003
F1	Glued	175	275	---	0.09	0.12	---
F02	Integral	1.0	1.5	1.3	0.002	0.002	0.002
F2	Glued	7.9	9.8	---	0.001	0.001	---

Table 5. Extracted viscous damping values of the diagonal elements C^a_{FyOUT} and $C^a_{Q\theta OUT}$.

equations for three other elements are developed and a set of equations is then used to find the entire matrix $\mathbf{C}_{\mathrm{OUT}}(\omega)$ from $\widetilde{\mathbf{K}}^{d}_{\mathrm{OUT}}(\omega)$ using SIM, EXP or FEM models.

$$\begin{Bmatrix} i\omega_{\min}\mathrm{C}_{\mathrm{FyOUT}}(\omega) \\ i\omega_{\min+1}\mathrm{C}_{\mathrm{FyOUT}}(\omega) \\ \vdots \\ i\omega_{\max}\mathrm{C}_{\mathrm{FyOUT}}(\omega) \end{Bmatrix} = \begin{Bmatrix} \mathrm{Im}[\widetilde{\mathrm{K}}^{d}_{\mathrm{FyOUT}}(\omega_{\min})] \\ \mathrm{Im}[\widetilde{\mathrm{K}}^{d}_{\mathrm{FyOUT}}(\omega_{\min+1})] \\ \vdots \\ \mathrm{Im}[\widetilde{\mathrm{K}}^{d}_{\mathrm{FyOUT}}(\omega_{\max})] \end{Bmatrix} \quad (39)$$

From measured ς_r, $\mathbf{C}_{\mathrm{OUT}}(\omega)$ of dimension 2×2 can be constructed in two steps. First, a proportional viscous damping matrix $\mathbf{C}_{\mathrm{IN}}(\omega)$ of dimension 4×4 is constructed using ς^1 and ς^2, and equation (27), as described before. For D0 constructed $\mathbf{C}_{\mathrm{IN}}(\omega)$ using equation (27) is as

$$\mathbf{C}_{\mathrm{IN}} = \mathbf{C}_{\mathcal{J}\mathrm{IN}} = \left[\begin{array}{cc:cc} 1.5 & 0.06 & -1.5 & 0.06 \\ 0.06 & 0.033 & 0.06 & 0.029 \\ \hdashline -1.5 & -0.06 & 1.5 & -0.06 \\ 0.06 & 0.029 & -0.06 & 0.033 \end{array}\right] \quad (40)$$

The sign convention in $\mathbf{C}_{\mathrm{IN}}(\omega)$ is the same as $\mathbf{K}^{s}_{\mathrm{IN}} = \mathbf{K}^{s}_{E}$ and relative magnitudes of elements follow similar trends in both "input" matrices. Similarly, proportional viscous damping matrices are derived for E1-E5, F01, F02, F1 and F2. Measured damping ratios (ς^1 and ς^2) for all examples are listed in [18].

Second, $\mathbf{C}_{\mathrm{IN}}(\omega)$ is used in equation (41), to obtain $\mathbf{C}_{\mathrm{OUT}}(\omega)$, as explained below.

$$\widetilde{\mathbf{D}}(\omega) = -\omega^2\mathbf{M} + \mathbf{K}^{s}_{J}(\omega) + i\omega\mathbf{C}_{J}(\omega) \quad (41)$$

Employing the system matrix $\widetilde{\mathbf{D}}(\omega)$ in this form, $\widetilde{\mathbf{H}}_{41}(\omega)$ is obtained using equation (18), and $\widetilde{\mathbf{K}}^{d}_{J}(\omega) = \widetilde{\mathbf{K}}^{d}_{\mathrm{OUT}}(\omega)$ from equation (7). The $\widetilde{\mathbf{K}}^{d}_{\mathrm{OUT}}(\omega)$ matrix follows the form of equation (38) from which $\mathbf{C}_{\mathrm{OUT}}(\omega)$ is obtained using equation (39). In a similar fashion, using measured ς^1 and ς^2 in FEM models, the most complex valued $\widetilde{\mathbf{K}}^{d}_{\mathrm{OUT}}(\omega)$ is found using ANSYS [18] and ultimately $\mathbf{C}_{\mathrm{OUT}}(\omega)$.

Since $\mathbf{C}_{\mathrm{OUT}}(\omega)$ is now available from SIM model, FEM and EXP models are compared with each other and with $\mathbf{C}_{\mathrm{IN}}(\omega)$. Results for D0 are displayed in Figure 9. In extracted damping spectra, frequency peaks for SIM and FEM results can be observed. Also, elements $\mathrm{C}_{\mathrm{FyOUT}}(\omega)$ (1,1), $\mathrm{C}_{\mathrm{FzOUT}}(\omega)$ (1,2), $\mathrm{C}_{\mathrm{QyOUT}}(\omega)$ (2,1) and $\mathrm{C}_{\mathrm{QzOUT}}(\omega)$ (2,2), show asymptotic lines at high frequencies. The values of $\mathbf{C}_{\mathrm{OUT}}(\omega)$ obtained from measured FRFs are quite high for both examples, though the spectrum is a straight line at the asymptote. Such a difference in magnitudes could be attributed to poor signal to noise ratios in experiments, different plausible arrangements of springs or viscous dampers. The viscous damping measured using EXP model is not discussed here. But a strong agreement between SIM, FEM and $\mathbf{C}_{\mathrm{IN}}(\omega)$ damping spectra is noticed. To quantify the values of each element of damping matrix $\mathbf{C}_{\mathrm{OUT}}(\omega)$, a spectral average of each element within the frequency range is carried out as given by equation (42). This new, frequency-invariant, proportional viscous damping matrix is labeled as $\mathbf{C}^{a}_{\mathrm{OUT}}$.

$$\mathrm{C}^{a}_{\mathrm{OUT}} = \left\langle \mathrm{C}_{\mathrm{OUT}}(\omega) \right\rangle_{\omega} = \frac{\sum_{1}^{\mathrm{n}} \mathrm{C}_{\mathrm{OUT}}(\omega)}{\mathrm{n}} \quad (42)$$

The frequency range ($\mathrm{f}_{\min}$ to $\mathrm{f}_{\max}$) is chosen such that the viscous damping spectrum is almost a straight line. Values of each element of $\mathbf{C}^{a}_{\mathrm{OUT}}$ are calculated for all examples. Diagonal elements are displayed in Table 5 and the off-diagonal elements are given in Table 6. Consistent results are obtained for all elements.

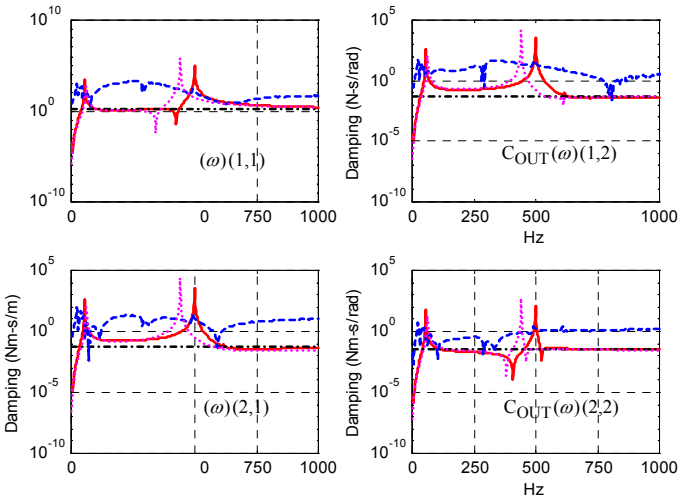

Figure 9. Proportional viscous damping spectra $\mathbf{C}_{\mathrm{OUT}}(\omega)$ for D0. Key: ——— SIM, ····· FEM, - - - - EXP and – · – · – C_{IN}

CONCLUSION

A frequency domain decomposition technique is successfully implemented to extract lumped static stiffness and proportional viscous damping matrices of elastic joints from an assembled structure using analytical (SIM), computational (FEM) or experimental (EXP) methods. For the integral joint examples, joint

static stiffness spectra from EXP model match well with SIM and FEM results. The decomposition technique is successfully applied to welded and glued joint assemblies. Example E5 is found to have the stiff shear and rotational stiffness elements. Example E2 is the most compliant for shear stiffness and E1 has the most compliant rotational stiffness element. Similarly, stiffness elements for glued joints are compared with the integral joint elements. Assembly viscous damping matrices are constructed and from that joint damping matrices are extracted. Asymptotic values of simulated and computed damping spectra match very well with each other and with the input viscous damping matrix. Future work should focus on multiple joints, as well as on the application of decomposition technique to real-life automotive structures.

ACKNOWLEDGMENTS

We are grateful to the Edison Welding Institute (EWI) and the Center for Automotive Research (CAR) Consortium for financially supporting this research. Special thanks go to Dr. Jeff Cropmton of EWI for his suggestions and help in fabricating welded fixtures. We would like to also thank Dr. Mayank Tiwari and Matt Young for their work during the earlier phase of the project.

REFERENCES

1. M. Kamal and J. Wolf, Modern Automotive Structure Analysis, Van Norstrand Reinhold Company, 1982.
2. Y. Ren and C.F. Beards, "On the Nature of FRF Joint Identification Technique", Proceedings of the 11th International Modal Analysis Conference, V 1(of 2) pp. 473-478, 1993.
3. M. Young, Identification of joint Stiffnesses Using a Component Synthesis Technique, M.S. Thesis, The Ohio State University, 2000.
4. J.H. Wang and C.M. Liou, "Experimental Identification of Mechanical Joint Parameter", ASME Journal of Vibration and Acoustics, V. 113, pp. 28-36, 1991.
5. Y. Ren and C.F. Beards, "On the Importance of Weighting for FRF Joint Identification", Proceedings of the 11th International Modal Analysis Conference, V. 1(of 2), pp. 1606-1611, 1993.
6. Y. Ren and C.F. Beards, "An Iterative Joint Identification Technique", Proceedings of the 11th International Modal Analysis Conference, V. 1(of 2), pp.1133 –1139, 1993.
7. W. Liu and D.J. Ewins, "Substructure Synthesis via Elastic Media. Part I: Joint Identification", International Modal Analysis Conference, pp. 1153-1159, 2000.
8. W. Liu and D.J. Ewins, "Substructure Synthesis via Elastic Media. Part II: Coupling Analysis", International Modal Analysis Conference, pp. 1153-1159, 2000.
9. S.Y. Chen, M.S. Ju and Y.G. Tsuei, "Estimation of Mass, Stiffness and Damping Matrices from Frequency Response Functions", Journal of Vibration and Acoustics, V. 118, pp. 78-82, 1996.
10. T.P. Gialamas, D.T. Tsahalis, D. Otte, H. Van der Auwaraer and D.A. Manolas, "Substructuring Technique: Improvement by Means of Singular Value Decomposition (SVD)", Applied Acoustics, V. 62, pp. 1211-1219, 2001.
11. Y. Liu, T. C. Lim and Y. Wang, Vibration Characteristics of Welded Beam and Plate Structures, Noise Control Engineering Journal, V. 49 (6), pp. 265-275, 2001.
12. LMS International <www.lmsintl.com>.
13. The Hewlett-Packard Company <www.hp.com>.
14. Agilent Technologies <www.agilent.com>.
15. The Mathworks <www.mathworks.com>.
16. The Waterloo Maple Inc. <www.maplesoft.com>.
17. ANSYS Inc. <www.ansys.com>.
18. P. Mehta and R. Singh, Effect of Welded or Glued Joints on Modal Properties of an Assembly, SAE paper # 03NVC-253.
19. R. Singh, Structural Mobility, Short Course for Delphi Chassis, pp. 53-58, 1999.
20. R. Singh, The Ohio State University ME 777 Course Notes, pp. 161-163, 1999.
21. ANSYS Theory Reference, Software Manuals, 11th edition, pp. 15.55-15.59
22. R. Singh, The Ohio State University, ME 778 Course Notes, pp. 44-88, 228-286, 2000.

Example	Type	Asymptotic viscous damping of off-diagonal elements of $\mathbf{C}_J^{sa} = \mathbf{C}_{\text{OUT}}^{sa}$					
		$C^a_{F\theta OUT}$ (kN/rad) (1,2)			C^a_{QyOUT} (kNm/m) (2,1)		
		C_{IN}	SIM	FEM	C_{IN}	SIM	FEM
D0	Integral	0.06	0.05	0.06	0.06	0.05	0.03
E1	Welded	0.1	0.2	0.07	0.1	0.2	0.06
E2		0.06	0.05	0.04	0.06	0.05	0.02
E3		0.05	0.07	0.05	0.05	0.07	0.05
E4		0.08	0.09	0.05	0.08	0.09	0.03
E5		0.03	0.02	0.03	0.03	0.02	0.03
F01	Integral	0.1	0.2	0.1	0.1	0.2	0.2
F1	Glued	2.2	3.2	---	2.2	3.2	---
F02	Integral	0.01	0.01	0.008	0.01	0.01	0.006
F2	Glued	0.01	0.1	---	0.01	0.1	---

Table 6. Extracted viscous damping values of the off-diagonal elements $C^a_{F\theta OUT}$ and C^a_{QyOUT}.